Hyperfine Interactions (2020) 241:10
https://doi.org/10.1007/s10751-019-1664-x

Magnetization and room temperature Mössabuer studies of $_{50}Fe_2O_3$-$_{50}SiO_2$ and $_{90}Fe_2O_3$-1_0SiO_2 ceramic fibers processed by laser floating zone method

Ali Salehizadeh[1] · Nuno M. Ferreira[2] · Manuel A. Valente[2] · Benilde F. O. Costa[3]

Published online: 16 December 2019

Abstract
In this work, we employed the Laser Floating Zone (LFZ) method to grow the ceramic fibers with composition of $_{50}Fe_2O_3$-$_{50}SiO_2$ and $_{90}Fe_2O_3$-$_{10}SiO_2$, with two different pulling rates: 25 and 200 mm/h. The physical properties of the ceramics were studied as the function of the iron oxide content and the pulling rate. XRD analysis depicted that the main crystalline phase formed in all samples is magnetite. Although, the appearance of small quantity of nano-crystalline fayalite was also confimed. From the magnetic measurements, a Verwey transition for all LFZ fibers in the temperature range varying from 100 to 115 K depending on the composition and the pulling rate, was observed. Room temperature 57-Fe Mössbauer measurements showed that the degree of non-stoichiometry of LFZ ceramics with 90% of the iron content is higher than one for LFZ samples containing 50% of iron oxide. A great agreement was obtained between the result of Mossbauer spectroscopy measurements and VSM studies. The revealed behaviours can be described in terms of the temperature dependent interactions occurring between the magnetic clusters formed in the fibres.

Keywords Laser floating zone method · Iron oxide-silica ceramics · Magnetite · Mössbauer spectroscopy · Non-stoichiometry

This article is part of the Topical Collection on *Proceedings of the International Conference on the Applications of the Mössbauer Effect (ICAME2019), 1-6 September 2019, Dalian, China*
Edited by Tao Zhang, Junhu Wang and Xiaodong Wang

✉ Benilde F. O. Costa
benilde@ci.uc.pt

[1] SEG-CEMMPRE, Mechanical Engineering Department, University of Coimbra, 3030-788 Coimbra, Portugal

[2] i3N - Department of Physics, University of Aveiro, 3810-193 Aveiro, Portugal

[3] CFisUC, Physics Department, University of Coimbra, P-3004-516 Coimbra, Portugal

1 Introduction

Iron oxide containing silica ceramic systems have achieved great importance in a wide range of industrial applications including metals extraction technologies [1], steelmaking processes and pyrometallurgical applications [2–5]. It is well-known that the laser floating zone (LFZ) method is the ideal approach to process the oxide ceramics [6, 7]. Among other high-temperature ceramic processing techniques, LFZ possesses several superiorities including suitable to work under non-equilibrium conditions, control of the crystallization/vitrification degree in the material, tuning the states of the redox-active cations and providing circumstances for a self-supported molten zone. Therefore, experimental difficulties due to high-temperature interaction with crucibles or other materials will be neglected [7–9]. In the specific case of the silica-based composites containing iron ions produced by LFZ technique, several literatures have shown that the iron ions present both oxidation states, 2+ and 3+, in the final produced ceramics [8]. However, it was revealed that the ratio of Fe^{2+}/Fe^{3+} and corresponding redox mechanism occurring during the sample processing are significantly influenced by the working conditions such as temperature, oxygen partial pressure, addition of a dopant, pulling rate, iron content in the starting composition and the oxidation state of iron ions in the initial powder mixture, i.e. using hematite or magnetite as the raw powder. These factor results in the formation of several iron oxide crystalline phases for example Fe_3O_4, α-Fe_2O_3, wustite along with others, with different size, shape and degree of stoichiometry and consequently impact on the structural, morphological, magnetic, and other physico-chemical properties [7–10]. It was found the Mössbauer spectroscopy is the most useful tool to identify truly the magnetic interaction taking place in the iron oxide bearing compositions and exact determination of the iron coordination environment and the fraction of each cation in the ceramic [8]. Our previous studies showed that incorporation of low content of iron oxide (less than 10% in mol) into the silica-based ceramic glasses prepared by LFZ method, does not provide any significant magnetic properties [8, 9] and only presents paramagnetic attribute at room temperature due to poor clustering of iron species and huge directional crystallization of non-magnetic components. Altough, the silica based ceramics doped by 10–15% concentration of iron oxide [7] present superparamagnetic-like character iron oxide likely because of matrix iron ions nucleation and clustering formation. Moreover, our attempts to grow fibers with $_{20}Fe_2O_3$-$_{85}SiO_2$, and $_{25}Fe_2O_3$-$_{80}SiO_2$ starting compositions, were not successful. The reason for this failure is still open to question. Here we investigate the structural, magnetic and Mössbauer characteristics of the ceramic fibers with the compositions of, $_{50}Fe_2O_3$-$_{50}SiO_2$ and $_{90}Fe_2O_3$-$_{10}SiO_2$, successfully grown at two different rates, 25 and 200 mm/h, by LFZ method. The aim of the work is to analyse the effects of pulling rate and iron oxide concentration on the corresponding properties of the fibers.

2 Experimental Procedure

According to the molar compositions of $_{50}Fe_2O_3$-$_{50}SiO_2$ and $_{90}Fe_2O_3$-$_{10}SiO_2$, the raw powders (MERCK, with >99.0% purity) were weighed and after mixed inside an agate container of a planetary ball milling system for 40 min at 250 rpm. After that, an organic binder (PVA –

Polyvinyl alcohol) was added to the mixture and the precursor rods were obtained from cold extrusion to be used as feed and seed precursors for the sample growth by the LFZ method.

The sample processing was carried out in the LFZ setup [6], equipped with a continuous with a continuous CO_2- Spectron SLC laser ($\lambda = 10.6$ μm; 200 W) in the air atmosphere. The rod diameter was kept at 1.75 mm, each composition was grown at two rates of 25 and 200 mm h^{-1} to yield dense glass-ceramics. Hereafter, the glass-ceramic fibers are labeled as xLFZy (x = 50, 90 and y = 25, 200) in which x and y mean the content of iron oxide in the glass ceramic and the pulling rate of each sample, respectively. Therefore, the fibers are denoted as 50LFZ25, 50LFZ200, 90LFZ25, and 90LFZ200 respectively.

X-ray diffraction (XRD) was performed using an X'Pert MPD Philips diffractometer (Cu Kα radiation, $\lambda = 0.154056$ nm, $2\theta = 15–70°$, step 0.04° and exposition 1.3 s) at 40 kV and 30 mA, and the obtained spectra were analyzed using the Joint Committee on Powder Diffraction Standards (JCPDS) database.

Microstructures were observed by a TESCAN VEGA3 SBH scanning electron microscope, operating at 20 kV and equipped with an EDS detector Burker XFlagh 410 M, which allowed the detection of the characteristic X-rays emitted by the sample and, consequently, the identification of its chemical elements. For the analysis, a small amount of the powder of the compounds was deposited on a carbon tape.

The magnetic susceptibility measurements were performed using a vibrating sample magnetometer (VSM) from Cryogenics. The magnetic properties as a function of temperature were acquired in field cooling (FC) and zero field cooling (ZFC) modes, applying a magnetic field of 0.1 Tesla on LFZ grown fibers, and magnetization versus magnetic field in the wide range of temperatures between 5 and 300 K. The magnetic measurements were made by placing the samples in the parallel position relative to the direction of the applied magnetic field.

Mössbauer spectra were recorded at room temperature by a constant acceleration type spectrometer (WissEL) in transmission geometry, using the ^{57}Fe as isotope and a source of ^{57}Co (energy of 14.4 keV) in a matrix of Rh with an activity of about 20 mCi. The spectra were fitted by a set of Lorentzian lines determined by the least square's method, applying the NORMOS program distributed by WissEL GmbH. Isomer shifts are given, as usually, relatively to α–Fe measured at room temperature.

3 Results and discussion

The XRD patterns of the LFZ samples were normalized in respect to the most intensive peak of each pattern and are given in Fig. 1a and b. It is revealed that the prominent lines correspond to the crystalline spinel ferrite phase of magnetite, Fe_3O_4 for all samples. Although some impurities regarding to fayalite, Fe_2SiO_4, crystalline phase were detected in the XRD patterns of LFZ ceramics. Moreover, the appearance of a weak and low intense peak related to α-Fe_2O_3 was confirmed in 90LFZ samples, being more evident in 90LFZ25. The formation of secondary phases in the ceramic fiber may cause the lattice distortion due to the defects such as vacancies, interstitials and non-stoichiometry resulting in the strain in crystal and induce the shift in XRD peak position. As observed in the insets of Fig. 1a and b, the most intense peak occurs at around $2\theta = 35.5^o$. This peak shifts slightly toward higher angles with increasing the pulling rate from 25 to 200 mm.h^{-1} in 50LFZ samples. While the peak position shifts to lower angles 90LFZ as the pulling rate rises up. In addition, there is a shoulder-like feature in the

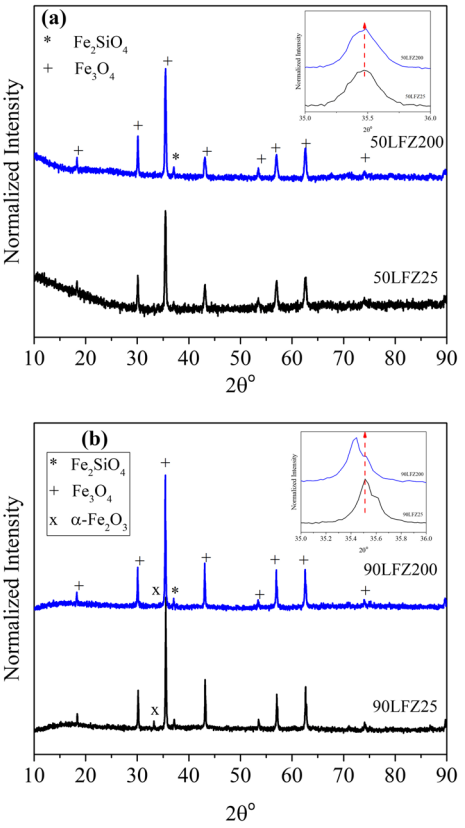

Fig. 1 XRD patterns of **a**) 50LFZ and **b**) 90LFZ fiber ceramics

most intensive line of 90LFZ samples which might be due to lattice deformation arising from more impurities formed in these samples. The observed shift can be indicative of the type of strain i.e., tensile and compressive strain in our samples [11]. We have employed the Williamson-Hall approach to determine precisely both crystallite size and strain contributions in the X-ray diffraction peak broadening which is expressed as [12]:

$$\left(\frac{\beta^*}{d^*}\right)^2 \approx \frac{1}{< D >_{W-H}} \frac{\beta^*}{(d^*)^2} + \left(\frac{\eta}{2}\right)^2 \quad (1)$$

where $<D>_{W\text{-}H}$ stands for the average apparent diameter and η represents the mean value of the strain. Here $\beta^* = \beta \cos\theta/\lambda$ and $d^* = 2\sin\theta/\lambda$. β and d* are the integral breadth and the interplanar distance, respectively. According to Eq. 1, the $<D>_{W\text{-}H}$ and η values of the LFZ samples were calculated and are enlisted in Table 1. According to Table 1, it is observed that the $<D>_{W\text{-}H}$ of 50LFZ25 has the biggest value among.

It is worth mentioning that the negative value of the intercept found from the W-H plot linearization revealed the presence of compressive strain in 90LFZ25 [13]. From Table 1 we can see that the strain value of 50LFZ25 is larger than the one for 50LFZ200. Furthermore, if the pulling rate is kept constant at 200 mm/h the strain values decreases with increasing of the iron oxide concentration. Since Fe^{3+} ions coexist with Fe^{2+} ions in Fe_3O_4 and the ionic radii of

Table 1 The structural and magnetic features obtained from the XRD, VSM and Mossbauer measurements of LFZ fibers (**All measurement are with ±1% error)

Sample	Grain Size (nm)	T_V (K)	Coercivity @ RT (T)	M_S @ RT (emu.g^{-1})	Strain	Degree of Non-Stiochiometry	Fe^{2+}/Fe^{3+} ratio
50LFZ25	114	114.18	0.017	75.19	0.00267	0.034	1.53
50LFZ200	53	114.52	0.023	68.44	0.00183	0.004	1.92
90LFZ25	47	101.18	–	92.28	–	0.047	1.38
90LFZ200	80	105.69	–	93.59	0.00149	0.040	1.45

Fe^{2+} is larger than the one of Fe^{3+} ions by about 10%, the ratio of Fe^{2+}/Fe^{3+} would be determining factor in the type and the magnitude of the strain, as already reported [14]. Mössbauer spectroscopy is found be to be a well-known method to extract exactly this ratio which will be discussed in the following.

Figure 2 shows characteristic SEM images of samples 50LFZ and 90LFZ ceramic fibers, where the morphology of the particles can be observed. As seen in the images, the size of the

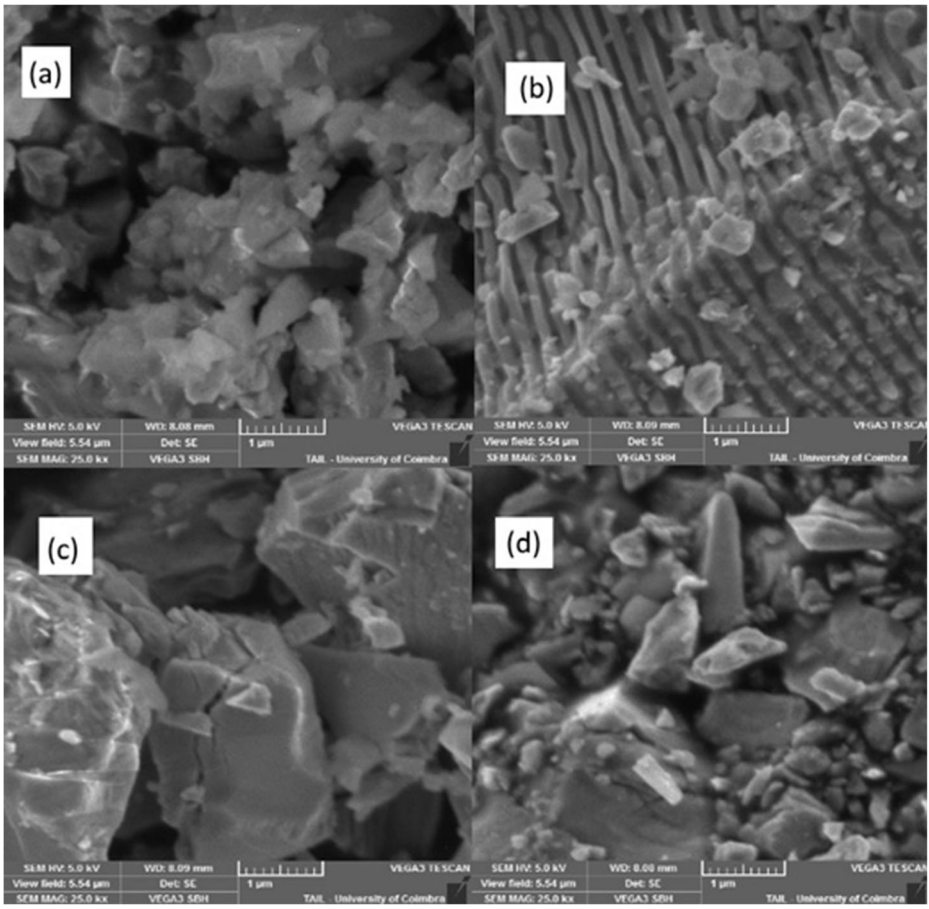

Fig. 2 SEM images of (**a**) 50LFZ25, (**b**) 50LFZ200 (**c**) 90LFZ25, and (**d**) 90LFZ200

particles decreases with increasing pulling rate for 50LFZ samples, in agreement with the XRD study.

The particles have the shape of parallelepipeds with sharp nozzles, except for the sample 50LFZ200, where small particles with the shape of strings of 0.2 μm width can be found.

Figure 3 presents the magnetization variation of the LFZ fibers as a function of the temperature in both ZFC and FC modes. There is a sharp and clear increase in the magnetization attributed to Verwey transition due to the magnetite crystalline ranging from 85 to 120 K depending on the composition. The Verwey transition temperature, T_V, in the case single phase and stoichiometric magnetite bulk crystalline phase is found to be around 124 K and this value can be deduced from the ZFC magnetization derivative, $dM_{(ZFC)}/dT$ [15]. It was reported that the T_V value is strongly sensitive to the size and shape, the method of synthesis and the degree of stoichiometry of the magnetite phase [16].

The derivative of the magnetization curve in ZFC mode were carried out for all samples and the obtained values of T_V are tabulated in Table 1. From Table 1 it is realized that the T_V values of the 50LFZ fiber are higher than one for 90LFZ ceramics and closer to the characteristic T_V value, 124 K, of the stoichiometric Fe_3O_4 phase. Also, the T_V value increases with the pulling rate for 90LFZ samples while the it does not change significantly with pulling rate variation for 50LFZ fibers.

Figure 4 demonstrates the magnetization loops of the LFZ sample recorded at 10 K and the room temperature, RT. Some parameters of LFZ samples, the coercivity, B_C, at room temperature and saturation magnetization at RT, are taken form the hysteresis loops and present in Table 1. It is obvious to see that the magnetizations of 90LFZ samples is greater than one for

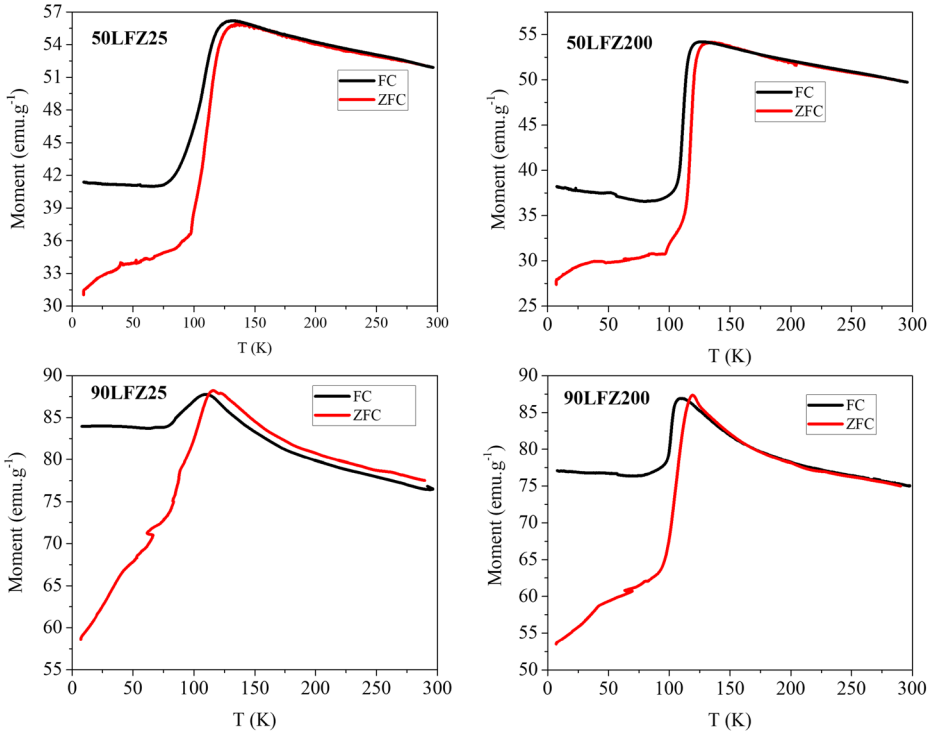

Fig. 3 ZFC-FC curves of the LFZ ceramics

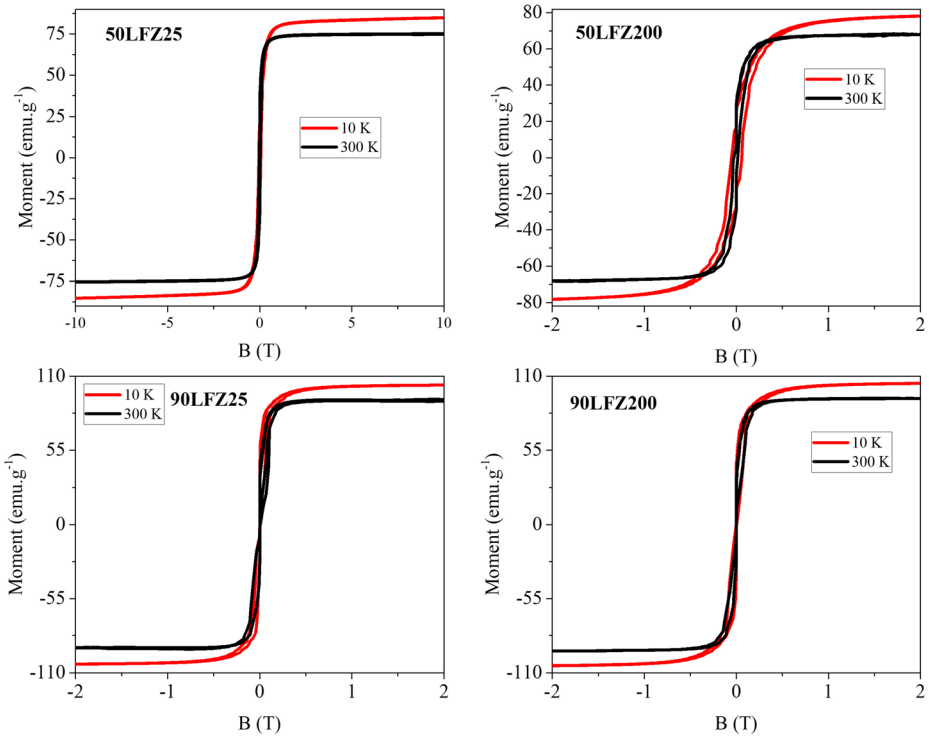

Fig. 4 the M(B) loops of all LFZ fibers, measured at 10 K and 300 K.

LFZ50 samples because of the existence of higher quantity of magnetite phase in these fibers. In addition, no corecivity was seen in the M-B loops of 90LFZ ceramics measured at RT, while the B_C values at RT decreases with reduction in the pulling rate for 50LFZ samples.

Figure 5 shows characteristic Mössbauer spectra of the samples taken at RT. The hyperfine parameters resulted from the spectra fitting procedures are shown in Table 2. Magnetite is found in all the spectra. During the sample's preparation, within heating temperature, hematite is transformed in magnetite which has a spinel structure. Magnetite has an inverse-spinel structure in which A sites (40%) (tetrahedral) are occupied by Fe^{3+} ions and B sites (60%) (octahedral sites) by Fe^{2+} and Fe^{3+} ions [17]. In addition, small percentage of fayalite, a paramagnetic substance at RT, which was detected in the XRD spectra being masked by the magnetic contributions of magnetite.

Non-stoichiometric magnetite is characterized by the presence of vacancies at octahedral sites and can be represented as [18]:

$$\left(Fe^{3+}\right)_A \left(Fe^{2+}{}_{1-3x}\right) \left(Fe^{3+}{}_{1+2x}\ \delta_x\right)_B O_4 \qquad (2)$$

where A and B are the tetrahedral and octahedral sites, respectively and δ is a vacancy.

The degree of non-stoichiometry ($_X$) can be determined from the area ratio of the sextets corresponding to Fe ions in A and B sites using [19]:

$$x = (2-r)/(6+5r) \qquad (3)$$

where $r = A_B/A_A$; A_A and A_B being the area of sextets corresponding to A and B sites.

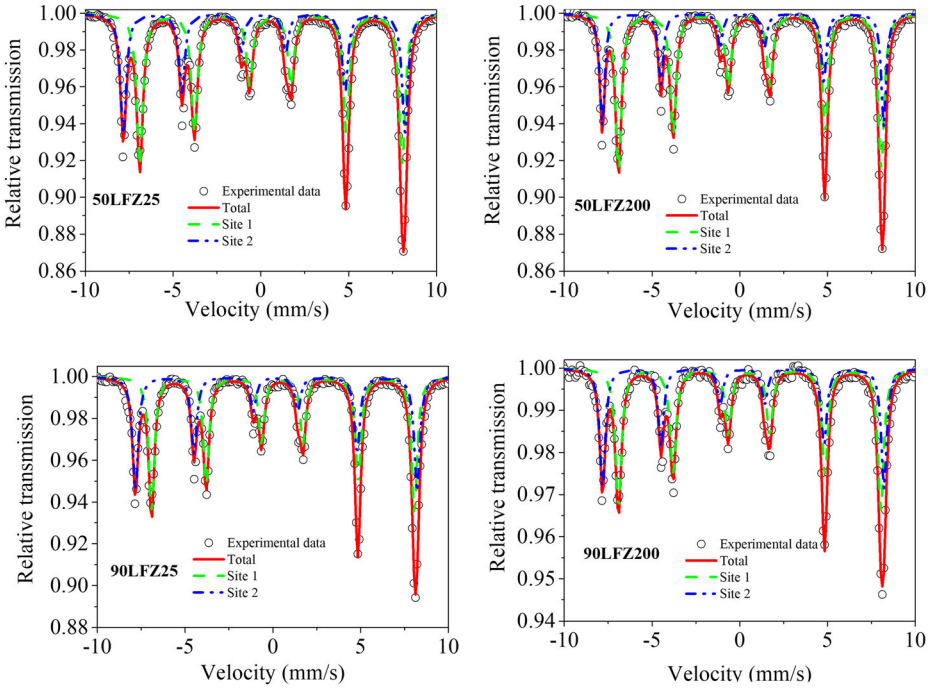

Fig. 5 RT Mössbauer spectra of all LFZ samples

According to Table 1, our samples are non-stoichiometric, but the degree of non-stoichiometry is higher in the case of the 90Fe/10Si samples and increases with increasing pulling rate. Magnetite is almost stoichiometric in the case of the 50Fe/50Si samples. This finding is in good agreement with the VSM and XRD analyses of our samples. The T_V value strongly depends on the degree of non-stoichiometry of the sample. As seen in Table 1, the most stoichiometric sample, 50LFZ200 has a T_V value of 114.52, closest to the characteristic T_V among all other samples. On the other hand, the lowest Fe^{2+}/Fe^{3+} ratio was found to be for 25LFZ90 which demonstrated a

Table 2 Hyperfine parameters obtained from the fitting of the RT spectra taken to the samples. Isomer shifts (IS) are given relatively to α-Fe

Sample	IS (mm/s)	QS (mm/s)	B (T)	W (mm/s)	%	Site
50LFZ25	0.67(1)	(0.04)	46.3(1)	0.42(1)	60.5	Fe^{2+}
	0.28(1)	(0.04)	49.7(1)	0.39(1)	39.5	Fe^{3+}
50LFZ200	0.67(1)	(0.04)	46.4(1)	0.40(2)	65.8	Fe^{2+}
	0.28(1)	(0.04)	49.7(1)	0.33(1)	34.2	Fe^{3+}
90LFZ25	0.67(1)	(0.04)	46.4(1)	0.38(1)	58.0	Fe^{2+}
	0.29(1)	(0.04)	49.7(1)	0.40(2)	42.0	Fe^{3+}
90LFZ200	0.66(1)	(0.04)	46.3(1)	0.41(1)	59.3	Fe^{2+}
	0.98(1)	(0.04)	49.7(1)	0.38(1)	40.7	Fe^{3+}

IS- isomer shift; QS- quadrupole splitting; B- hyperfine magnetic field; W- full width at Lorentzian half maximum; %- percentage of site

QS was fixed in the fitting procedure, so it is written in brackets

compressive stain according to the XRD study. This implies our suggestion saying that the type of strain is not only influenced by the structural defect formation arisen from the impurities and interstitial deformation in the crystal lattice but also the Fe^{2+}/F^{3+} ratio in the composition.

4 Conclusion

In this study we investigate, the magnetic and structural characteristics of silica fibers bearing iron oxide, with two different concentrations: 50 and 90 in mol%, processed by LFZ method in the pulling rates of 25 and 200 mm.h-1. The physical properties of the ceramics were studied as the function of the iron oxide content and the pulling rate. From this study we could suggest that more Mössbauer measurements at different temperatures below 300 K are required in order to distinguish truly the magnetic interactions taking placing within the clusters formed in the LFZ ceramics.

Acknowledgments CFisUC is supported by funds from FEDER (ProgramaOperacionalFactores de Competitividade COMPETE) and from FCT-Fundação para a Ciência e a Tecnologia under the Project No. UID/FIS/04564/2016. Access to TAIL-UC funded under QREN-Mais Centro Project ICT-2009-02-012-1890, is gratefully acknowledged.

References

1. Wang, D., Gmitter, A.J., Sadoway, D.R.: Production of oxygen gas and liquid, metal by electrochemical. Decomposition of Molten Iron Oxide J. Electrochem. Soc. **158**(6), E51–E54 (2011)
2. Chankac, C., Tronc, E., Jolivet, J.P.: Thermal behavior of spinel iron oxide-silica composites. Nanostruct. Mater. **6**, 715–718 (1995)
3. Allanore, A.: Electrochemical engineering of anodic oxygen evolution in molten oxides. Electrochim. Acta. **110**, 587–592 (2013)
4. Mekki, A.: Magnetic properties of Fe ions in a silicate glass and ceramic. Phys. StatusSolidi A. **184**, 327–333 (2001)
5. Jung, I.H., Decterov, S.A., Pelton, A.D.: Critical thermodynamic evaluation and optimization of the FeO–Fe_2O_3–MgO–SiO_2 system. Metall. Mater. Trans. A. **B35**, 877–889 (2004)
6. Rey-García, F., Fernandes, A.J.S., Costa, F.M.: Influence of Lu content on $(Lu_xGd_{1-x})_2SiO_5$ oxyorthosilicates grown by laser floating zone: structural studies and transparency. Mater. Res. Bull. **112**, 413–419 (2019)
7. Ferreira N.M., Sarabando A.R, Atanasova-Vladimirova S., Kukeva R., Stoyanova R., Ranguelov B.S., Costa F.M., Ceramics International (2019) Iron oxidation state effect on the Mg-Al- Si-O glassy system https://doi.org/10.1016/j.ceramint.2019.07.125
8. Ferreira, N.M., Kovalevsky, A.V., Valente, M.A., Sobolev, N.A., Waerenborgh, J.C., Costa, F.M., Frade, J.R.: Iron incorporation into magnesium aluminosilicate glass network under fast laser floating zone processing. Ceram. Int. **42**, 2693–2698 (2016)
9. Ferreira, N.M., Kovalevsky, A., Valente, M.A., Costa, F.M., Frade, J.: Magnetite/hematite core/shell fibres grown by laser floating zone method. Appl. Surf. Sci. **278**, 203–206 (2013)
10. Ferreira, N.M., Ferro, M.C., Valente, M.A., Frade, J.R., Costa, F.M., Kovalevsky, A.V.: Unusual redox behaviour of the magnetite/hematite core–shell structures processed by the laser floating zone method. Dalton Trans. **47**, 5646–5651 (2018)
11. Kumari, R., Sahai, A., Goswami, N.: Effect of nitrogen doping on structural and optical properties of ZnO nanoparticles. Prog. Nat. Sci.: Mater. Int. **25**, 300–309 (2015)
12. Zamiri, R., Salehizadeh, S.A., Abbastabar, A.H., Shabani, M., Rebelo, A., Suresh, K.J., Soares, M.J., Valente, M.A., Ferreira, J.M.F.: Mater. Chem. Phys. **192**, 330–338 (2017)

13. Khorsand Zak, A., Majid, W.H.A., Abrishami, M.E., Yousefi, R.: X-ray analysis of ZnO nanoparticles by Williamson–Hall and size–strain plot methods. Solid State Sci. **13**, 251–256 (2011)
14. Sahai, A., Kumar, Y., Agarwal, V., Olive-Méndez, S.F., Goswami, N.: Doping concentration driven morphological evolution of Fe doped ZnO nanostructures. J. Appl. Phys. **116**, 164315 (2014)
15. Brollo, M.E.F., Lopez-Ruiz, R., Muraca, D., Figueroa, S.J.A., Pirota, K.R., Knobe, M.: Compact Ag@Fe3O4 core-shell nanoparticles by means of single-step thermal decomposition reaction. Sci. Rep. **4**, 6839 (2014). https://doi.org/10.1038/srep06839
16. Bohra, M., Agarwal, N., Singh, V.: A short review on Verwey transition in nanostructured Fe_3O_4 materials. J. Nanomater. (2019). https://doi.org/10.1155/2019/8457383
17. Gaspar, A.S., Wagner, F.E., Amaral, V.S., Costa Lima, S.A., Khomchenko, V.A., Santos, J.G., Costa, B.F.O., Durães, L.: Development of a biocompatible magnetic nanofluid by incorporating SPIONs in Amazonian oils. Spectrosc. Acta A: Mol. Biomol. Spectrosc. **172**, 135–146 (2017)
18. Kalska-Szostko, B., Wykowska, U., Satuła, D.: Core–shell and multilayered magnetite nanoparticles—structural and Mössbauer studies. Appl. Surf. Sci. **306**, 7–15 (2014)
19. Roychowdhury, A., Pati, S.P., Kumar, S., Das, D.: Effects of magnetite nanoparticles on optical properties of zinc sulfide in fluorescent-magnetic Fe_3O_4/ZnS nanocomposites. Powder Technol. **254**, 583–590 (2014)